

Field digitization scaling in a $\mathbb{Z}_N \subset U(1)$ symmetric model

Gabriele Calliari,* Robert Ott, Hannes Pichler, and Torsten V. Zache†

*Institute for Theoretical Physics, University of Innsbruck, Innsbruck, 6020, Austria and
Institute for Quantum Optics and Quantum Information,
Austrian Academy of Sciences, Innsbruck, 6020, Austria*

The simulation of quantum field theories, both classical and quantum, requires regularization of infinitely many degrees of freedom. However, in the context of field digitization (FD) – a truncation of the local fields to N discrete values – a comprehensive framework to obtain continuum results is currently missing. Here, we propose to analyze FD by interpreting the parameter N as a coupling in the renormalization group (RG) sense. As a first example, we investigate the two-dimensional classical N -state clock model as a \mathbb{Z}_N FD of the $U(1)$ -symmetric XY-model. Using effective field theory, we employ the RG to derive generalized scaling hypotheses involving the FD parameter N , which allows us to relate data obtained for different N -regularized models in a procedure that we term *field digitization scaling* (FDS). Using numerical tensor-network calculations at finite bond dimension χ , we further uncover an unconventional universal crossover around a low-temperature phase transition induced by finite N , demonstrating that FDS can be extended to describe the interplay of χ and N . Finally, we analytically prove that our calculations for the 2D classical-statistical \mathbb{Z}_N clock model are directly related to the quantum physics in the ground state of a (2+1)D \mathbb{Z}_N lattice gauge theory which serves as a FD of compact quantum electrodynamics. Our study thus paves the way for applications of FDS to quantum simulations of more complex models in higher spatial dimensions, where it could serve as a tool to analyze the continuum limit of digitized quantum field theories.

Introduction.— Quantum field theories (QFTs) are powerful theoretical descriptions of nature at all energy scales, ranging from condensed matter [1] to high-energy physics [2]. Solving QFTs is a long-standing, ongoing effort and has motivated developing extensive theoretical and numerical computing tools for classical simulations, e.g., with Monte Carlo sampling [3, 4] or tensor networks [5, 6], and more recently, quantum simulations using quantum hardware [7, 8]. A common challenge in all of these approaches is the regularization of the QFT’s infinitely many continuous degrees of freedom at a definite length (or energy) scale, and the task of obtaining regularization-independent results in the continuum limit.

Most prominently, quantum fields are discretized on finite lattices [4, 9], where thermodynamic and continuum results can be retrieved with a finite-size scaling analysis [10]. However, in addition to finite lattices, several simulation techniques — from quantum-inspired classical methods, such as tensor networks, to future large-scale quantum computation — typically require a digitization of the fields, which are locally truncated to finitely many values [11–14]. Removing this digitization to obtain physical continuum results, however, is challenging and further complicated in the presence of continuous symmetries, as is the case for lattice gauge theories (LGTs). While recently several such field-digitization strategies have been developed – for example based on finite subgroups [15–20], fixed representation cutoffs [21–26], orbifold constructions [27, 28], quantum groups [29–31], large- N_c expansions [32], quantum link models or large spins [33–39], qubit regularization [40–42], or Hamiltonian truncation [43] – a generally applicable framework for obtaining continuum limits, and a comprehensive understanding of these different procedures in terms of the

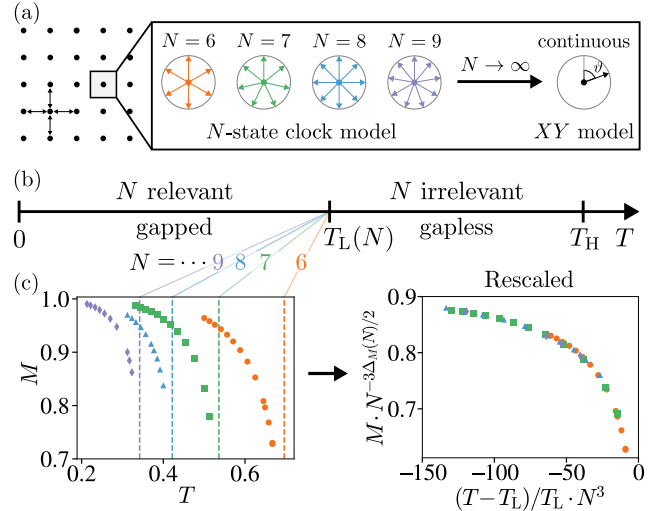


Figure 1. Field digitization scaling in the N -state clock model. (a) We investigate the N -state clock model with nearest-neighbor-interacting, discrete angles $\vartheta = 2\pi n/N$, ($n = 0, \dots, N-1$) on a 2D square lattice. In the limit $N \rightarrow \infty$, these \mathbb{Z}_N -symmetric models give rise to the $U(1)$ -invariant XY-model, which is gapless for $T < T_H$. (b) Field digitization to N discrete angles is relevant only at low temperatures, leading to an ordered, gapped phase at $T \leq T_L(N)$. (c) In this regime we uncover a self-similar scaling behavior among different N -regularized models. (Left) Magnetization M for different N versus temperature T . Dashed colored vertical lines represent $T_L(N)$. (Right) Based on the behavior of the correlation length $\xi(T, N)$ [see Eq. (5) and Fig. 2], we formulate an N -dependent scaling Ansatz [Eq. (6)] for local observables. Upon rescaling both axes accordingly, we observe a collapse of M for different N and T .

renormalization group (RG) are still missing.

In this letter, we take first steps towards an RG framework incorporating the truncation of the local field to a finite number (N) of values. Focusing on the example of digitizing the continuous group $U(1)$ to

* Gabriele.Calliari@uibk.ac.at

† Torsten.Zache@uibk.ac.at

a finite subgroup \mathbb{Z}_N , we show that it is possible to interpret the truncation parameter N as a coupling constant, and thus distinguish physical scenarios in terms of relevant or irrelevant field truncation. We probe this framework by systematically varying N in a scaling analysis: the *field digitization scaling* (FDS). We first demonstrate its applicability with tensor-network simulations of a two-dimensional classical \mathbb{Z}_N -symmetric clock model, a regularization of the continuous-field XY-model to N discrete angles [see Fig. 1(a)]. By the quantum-classical correspondence, our results also translate to the 1D quantum N -state clock model [44]. We show that for large enough N , rescaling the numerical data as a function of N and temperature T relates different N regularizations in an RG sense and allows us to retrieve results that are controlled by the continuous symmetry group $U(1)$. Furthermore, we extend our analysis to take into account the bond dimension χ of the tensor network, which plays the role of a second regulator. This motivates a novel generalized scaling Ansatz of N, T and χ , with which we uncover an unconventional crossover regime.

As a generalization, we demonstrate that our numerical results have direct consequences for quantum gauge theories. Specifically, we prove an explicit relation between our chosen tensor-network representation and the ground state of a (2+1)D \mathbb{Z}_N -symmetric LGT, which provides an asymptotic regularization of compact quantum electrodynamics. This indicates that our results apply to a much larger class of classical and quantum models, and our FDS analysis thus paves the way towards a more complete understanding of how to obtain continuum results from field-digitized models.

Field digitization.— As an example of a field-digitized model, we consider the N -state clock model (with $N > 5$ [45]), described by the Hamiltonian

$$H_N = -J \sum_{\langle ij \rangle} \cos(\vartheta_i - \vartheta_j), \quad \vartheta_i = \frac{2\pi n_i}{N}, \quad (1)$$

with $n_i = 0, \dots, N-1$, and $J = 1$ the coupling strength. Here, the degrees of freedom ϑ_i are digitized, $\mathbb{Z}_N \subset U(1)$ classical angles, interacting with their nearest-neighbors on a two-dimensional square lattice [see Fig. 1(a)]. This model has been extensively studied in the literature for various N [46–48], and in the limit $N \rightarrow \infty$ it reduces to the XY-model [49–51]. The partition function $Z(N, \beta)$ for an infinite system, where $\beta = 1/T$ is the inverse temperature, can be directly encoded in a 2D tensor network (see App. A)

$$Z(N, \beta) = \sum_{\{\vartheta_i\}} e^{-\beta H_N} = \text{[Tensor Network Diagram]} \xrightarrow{\chi \rightarrow \infty} \text{[Truncated Tensor Network Diagram]}. \quad (2)$$

As indicated on the right, we further regulate the infinite system with truncated environment tensors, representing the partition function $Z(N, \beta, \chi)$, which we obtain through the isotropic CTMRG algorithm [52]. This introduces the bond dimension χ , which, similar to a finite system size, truncates the correlations of the system. The full partition function is recovered as $Z(N, \beta, \chi) \xrightarrow{\chi \rightarrow \infty} Z(N, \beta)$.

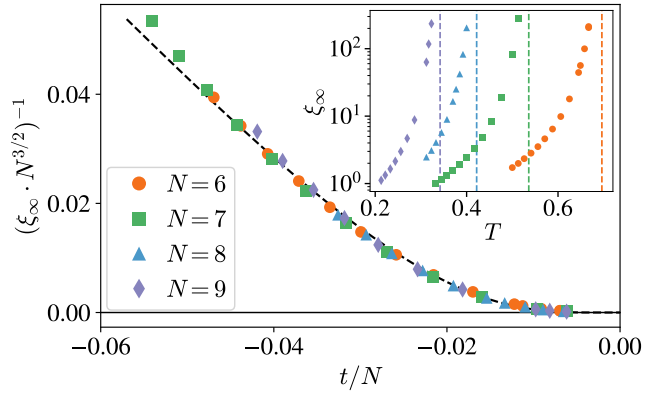


Figure 2. Relevant field digitization and universal behavior. In the gapped, ordered phase we uncover a universal scaling form of the correlation length. Shown is the extrapolated correlation length $\xi_\infty = \xi(\chi \rightarrow \infty)$ as a function of the reduced temperature $t = (T - T_L)/T_L$ for field dimensions $N = 6, 7, 8, 9$. Data points collapse on a single curve [dashed black line, see Eq. (5)] upon rescaling with N . (Inset) Unrescaled correlation length ξ_∞ versus temperature T . Colored vertical dashed lines represent $T_L(N)$.

To interpret the impact of the truncation parameter N from an RG perspective, we use an effective description in terms of continuous fields $\theta(x), \phi(x)$, with $x = (x_1, x_2)$ coordinates in two-dimensional Euclidean space. The field θ is the continuous-variable generalization of the microscopic variable ϑ , and the dual field ϕ obeys $\partial_\mu \phi = -\varepsilon_{\mu\nu} K \partial_\nu \theta$, where $\partial_\mu = \partial/\partial x_\mu$, $\mu = 1, 2$, and $K = K(T)$ is the Luttinger parameter. One can show that the expected low-energy effective action for the model H_N takes the form [53, 54]

$$S_N = S_{\text{sG}} + \frac{g_L}{2\pi\alpha^2} \int d^2x \cos(N\sqrt{2}\theta), \quad (3)$$

$$S_{\text{sG}} = \int d^2x \left\{ \frac{1}{2\pi K} (\nabla\phi)^2 + \frac{g_H}{2\pi\alpha^2} \cos(\sqrt{2}\phi) \right\}. \quad (4)$$

S_{sG} describes the Euclidean sine-Gordon (sG) field theory, with coupling constant $g_H = g_H(T, N)$ and UV-cutoff α , while $g_L = g_L(T, N)$ is the coupling constant of a dual cosine interaction generated by the truncation. The latter term explicitly depends on N , revealing that N plays the role of a coupling parameter. At temperatures $T > T_L$ the additional operator $\sim \cos(N\sqrt{2}\theta)$ is RG-irrelevant [see Fig. 1(b)], and we recover the standard sG theory, with a critical, gapless phase below T_H [55]. Conversely, for $T < T_L (< T_H)$, N induces a relevant perturbation, leading to an ordered, gapped phase, which is separated from the gapless phase by a Berezinskii-Kosterlitz-Thouless (BKT) transition at $T_L(N)$ [44, 56].

Field digitization as a relevant perturbation.— To demonstrate that the field digitization N can be interpreted as a relevant perturbation, we consider the correlation length ξ next. Specifically, we focus on the ordered phase $T < T_L$ in the vicinity of the critical point (CP), and investigate how the field digitization N affects the observables.

In particular, we relate the functional behavior of ξ to an RG analysis involving N . Below T_H the operator $\cos(\sqrt{2}\phi)$ is irrelevant, and S_N effectively reduces to a dual sG action. From the corresponding

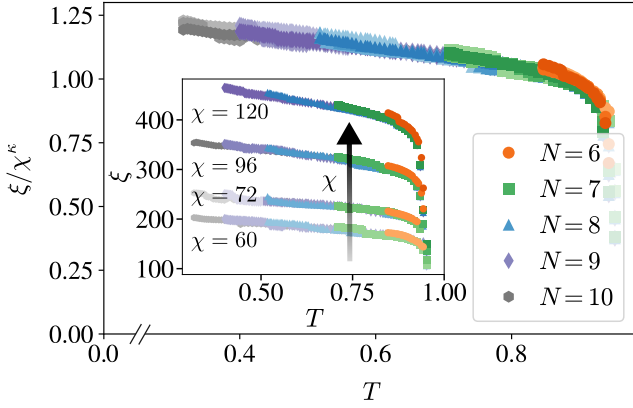


Figure 3. **Emergent $U(1)$ symmetry at finite N .** In the gapless, critical phase the field digitization N is an irrelevant perturbation: (Inset) the trivial collapse in N reveals the emergent $U(1)$ symmetry. Instead, the finite χ truncates the otherwise diverging correlation length ξ , shown versus T for different N and increasing bond dimension χ (increasing intensity). (Main) Upon rescaling the vertical axis as ξ/χ^κ , we observe a collapse for different χ and N as a function of temperature T .

RG flow equations [57], we derive that close to the CP the correlation length scales as $\xi \propto \exp\{\pi/(4 \cdot \sqrt{C})\}$, with $C \approx (g_L(T, N)/2\pi)^2$ (see App. B). We then explicitly determine the N -dependence in C and in the prefactor from our numerical simulations. Since the ordered phase is gapped, we can extrapolate the data points to the limit $\chi \rightarrow \infty$; our numerical results for $\xi_\infty = \xi(\chi \rightarrow \infty)$ indeed confirm the derived scaling with

$$\xi_\infty(T, N) = \frac{\varepsilon_0}{N^a} \exp\left(\frac{\pi}{4} \frac{1}{\sqrt{|t|/N^b}}\right), \quad (5)$$

where $a \approx 1.5$, $b \approx 1$, $\varepsilon_0 \approx \log(2)$ are consistent with our numerical results, while $t = (T - T_L(N))/T_L(N) < 0$ labels the distance from the CP (see Fig. 2)[58][59]. Therefore, our numerical simulation confirms the interpretation of the truncation parameter N as an RG coupling.

We now use the uncovered behavior of the correlation length ξ_∞ to make further predictions on the field digitization scaling of local observables. According to standard scaling arguments [10], close to the CP T_L an observable $O_\infty(T, N)$ with scaling dimension $\Delta_O(N)$ scales as $O_\infty(T, N) \sim \xi^{-\Delta_O(N)}$. Note that here the label “ ∞ ” indicates that the observable O is independent of χ , i.e., the regulator is removed. Based on Eq. (5), we can then formulate the scaling Ansatz

$$O_\infty(T, N) = N^{\frac{3}{2}\Delta_O(N)} f\left[\frac{|t|}{N \cdot \Delta_O^2(N)}\right], \quad (6)$$

with scaling function $f[x]$. We test our Ansatz for the extrapolated magnetization $M_\infty = M(\chi \rightarrow \infty)$, with $M = \cos(\vartheta_i)$, which translates to the operator $\cos(\sqrt{2}\theta)$ in the low-energy effective theory Eq. (3). As shown in Fig. 1(c), upon properly rescaling the numerical results according to Eq. (6) and with $\Delta_M = 2/N^2$, we obtain a collapse of the data points for different N and T , providing further evidence for our Ansatz.

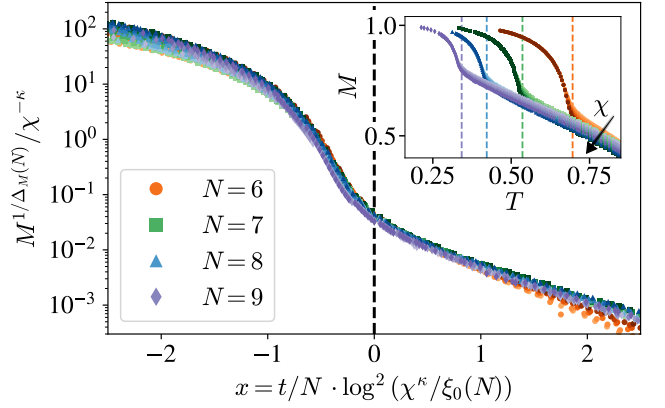


Figure 4. **Crossover regime.** Close to the CP $T = T_L$ both truncations in N and χ are relevant — rescaling according to Eq. (7) leads to a scaling collapse. (Main) Rescaled magnetization M is shown as a function of the parameter $x = t/N \cdot \log^2(\chi^\kappa/\xi_0(N))$ for several N (different colors and shapes) and bond dimension χ (increasing intensity, from $\chi = 60$ up to a maximum of $\chi = 192$ for $N = 6, 7$). (Inset) Unrescaled magnetization M versus temperature T . Vertical dashed lines represent $T_L(N)$. The black shaded arrow indicates increasing χ .

Note that, in contrast to standard scaling approaches, here the truncation parameter N also appears in the exponents through an N -dependent scaling dimension.

Irrelevant field digitization and emerging $U(1)$ -symmetry.— Let us now consider the regime in which the perturbation N is irrelevant, i.e., we focus on the gapless region ($T_L < T < T_H$). Deep in the critical phase, in agreement with predictions from the effective field theory, our numerical results confirm the expected collapse among different N — revealing the emergence of the $U(1)$ -invariance already at small values of N (see Insets of Fig. 3 and Fig. 4). In this regime the physics is captured by the Luttinger liquid conformal field theory (CFT). Due to the finite bond dimension χ , our tensor-network calculations introduce an additional relevant perturbation, which truncates the otherwise diverging correlation length as $\xi \propto \chi^\kappa$ (with κ a parameter fixed by the CFT, which we numerically extrapolate to $\kappa = 1.247$) [60, 61]. In agreement with previous observations [47, 54], the numerical data in this gapless phase depend on χ , yet upon rescaling the y -axis as ξ/χ^κ , we obtain a collapse for multiple N, χ and T (see Fig. 3). Close to the gapped ordered regime we observe some deviations in χ and N from the universal curve, which we attribute to the impact of the operator $\cos(N\sqrt{2}\theta)$ and its non-trivial interplay with the truncation in χ , which we study in detail next.

Crossover regime.— So far, we have separately investigated the effects of the regularizations introduced by N and χ on the two sides of the low-temperature phase transition. That is, we studied regimes sufficiently far away from the CP, where one of these perturbations dominates. Instead, we now focus on the region closer to the CP $T = T_L$ and investigate the interplay of N and χ , as well as of the temperature T . To capture their combined effect, we formulate a scaling Ansatz for general local observables $O = O(T, N, \chi)$.

To start, motivated by the uncovered behavior of $\xi_\infty(T, N)$ in Eq. (5), we introduce the scaling variable

$x = t/N \cdot \log^2(\xi/\xi_0(N))$, with $\xi_0(N) = \log(2)/N^{3/2}$, which by definition should remain constant in the critical regime. As shown in the previous section, the finite χ truncates the correlation length $\xi \sim \chi^\kappa$ and the observable $O \propto \xi^{-\Delta_O(N)} \sim \chi^{-\kappa\Delta_O(N)}$ in both the gapless phase and close to the CP [62]. In analogy with the scaling Ansätze for continuous phase transitions [60], we thus introduce a generalized scaling Ansatz

$$O(T, N, \chi) = \left(\chi^\kappa g \left[\frac{t}{N} \log^2 \left(\frac{\chi^\kappa}{\xi_0(N)} \right) \right] \right)^{-\Delta_O(N)}, \quad (7)$$

with scaling function $g[x]$. Note that for an N -independent scaling dimension Δ_O , we retrieve the usual scaling Ansatz $O(T, \chi) = \chi^{-\kappa\Delta_O} h[x]$, with the scaling function $h[x] = (g[x])^{-\Delta_O}$ [47, 60, 61].

We test our scaling hypothesis with the magnetization M , which at the CP has an N -dependent scaling dimension $\Delta_M(N) = 2/N^2$. As demonstrated in Fig. 4, rescaling the axes according to Eq. (7) leads to a scaling collapse around the CP for a wide range of values of N and χ , confirming the validity of our generalized Ansatz.

Generalizations.— Until here, our investigation has focused on an example of a 2D classical statistical model. However, the standard quantum-to-classical correspondence implies that our FDS analysis also applies to the 1D quantum clock model, where N represents the local Hilbert space dimension $\dim(\mathcal{H}) = N$. Throughout this work, we have used the fact that classical 2D models can also be encoded in 2D tensor-network states [63] suggesting a further extension to 2D quantum models. We thus expect that a similar analysis could be extended to other one- and higher-dimensional quantum models, where we believe our approach to have widespread consequences for the quantum simulation of models with (local) continuous-group internal symmetries, in particular lattice gauge theories.

As an example, we now relate the above 2D classical N -state clock model to a (2+1)D quantum \mathbb{Z}_N LGT. Specifically, consider the 2D quantum Hamiltonian

$$H_{\text{LGT}} = \frac{1}{2} \sum_p \left[(D_p(\beta) + D'_p(\beta)) - (U_p + U_p^\dagger) \right], \quad (8)$$

with plaquette operators $U_p = X_{p,1}X_{p,2}X_{p,3}^\dagger X_{p,4}^\dagger$ and $D_p^{(l)}(\beta) = \exp\{-(\beta/4)[\sum_{l=1}^4 c_l^{(l)} Z_{p,l} + \text{H.c.}]\}$ (see App. C, and for a sketch Fig. 5). Here, $c_l^{(l)}$ are judiciously chosen, N -dependent complex coefficients, β represents a coupling constant, which we eventually identify as the inverse temperature of the 2D classical model, while Z and X are N -dimensional clock and shift operators. Moreover, we restrict ourselves to gauge-invariant states, that is, we impose the Gauss' law constraints $G_s = Z_{s,1}Z_{s,2}Z_{s,3}^\dagger Z_{s,4}^\dagger = 1$ on all vertices s . In the limit $\beta \ll 1$, the operators $(D_p(\beta) + D'_p(\beta))/2$ simplify to $-\beta(1 - \cos(2\pi/N)) \sum_{l=1}^4 (Z_{p,l} + Z_{p,l}^\dagger)$, such that the Hamiltonian reduces to a standard \mathbb{Z}_N LGT [64], that we interpret as a field digitization of (2+1)D compact quantum electrodynamics.

In App. C, extending an analytical result from the $N = 2$ case [65] to arbitrary N , we prove that the

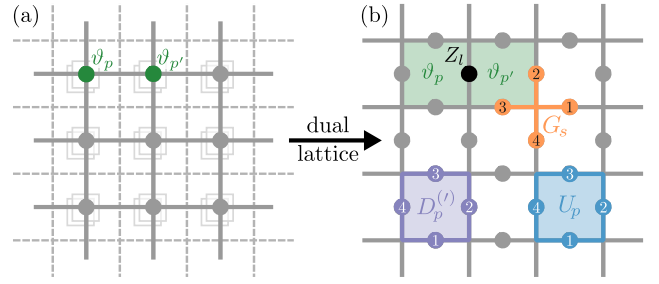


Figure 5. **Connecting the classical N -state clock model to a (2+1)D \mathbb{Z}_N LGT.** The tensor-network encoding of the 2D classical partition function Z_N [(a)] captures the quantum ground state of a \mathbb{Z}_N LGT with Hamiltonian given in Eq. (8) on the dual lattice [(b)]. (a) On each site p of a 2D lattice we define the microscopic, discrete angle ϑ_p [see Eq. (1)]. The partition function Z_N [Eq. (2)] on this lattice can be encoded in a 2D tensor network, as depicted in the background. The dashed lines represent the dual lattice, each site of which is mapped to a plaquette of the original lattice (and vice versa). (b) On the dual lattice we define plaquette $[U_p = X_{p,1}X_{p,2}X_{p,3}^\dagger X_{p,4}^\dagger]$ and Gauss' law operators $[G_s = Z_{s,1}Z_{s,2}Z_{s,3}^\dagger Z_{s,4}^\dagger]$, where the labels 1, ..., 4 refer to links near plaquettes p and vertices s as indicated. Similarly, we define the operators $D_p^{(l)} = f(Z_{p,l})$, with $l = 1, \dots, 4$ (see App. C). The operator Z_l on the link $l = \langle p, p' \rangle$ between two plaquettes p, p' is defined by ϑ_p and $\vartheta_{p'}$ as $Z_l \equiv \exp\{i(\vartheta_p - \vartheta_{p'})\}$.

ground state of the \mathbb{Z}_N LGT [Eq. (8)][66] is given by

$$|\vartheta\rangle = \sum_{\{\vartheta_p\}} e^{\frac{\beta}{2} \sum_{\langle p, p' \rangle} \cos(\vartheta_p - \vartheta_{p'})} g(\{\vartheta_p\}) |\Omega\rangle, \quad (9)$$

with $Z_\vartheta = \langle \vartheta | \vartheta \rangle = \sum_{\{\vartheta_p\}} e^{\beta \sum_{\langle p, p' \rangle} \cos(\vartheta_p - \vartheta_{p'})}$ being the corresponding partition function. Here, $|\Omega\rangle = \otimes_l |0\rangle$ is a trivial product state on the dual lattice, and ϑ_p are digitized, angular variables defined on sites p , associated with the plaquettes of the dual lattice. Applying the operators $g(\{\vartheta_p\}) = \prod_p (U_p)^{n_p}$, with $\vartheta_p = 2\pi(n_p \bmod N)/N$, on $|\Omega\rangle$ creates all possible gauge-invariant configurations. The ground state $|\vartheta\rangle$ can be directly encoded in a tensor network of finite bond dimension, which corresponds to the tensor network in Eq. (2), i.e., $Z_\vartheta = Z(N, \beta)$ (see also App. A) [63]. This identification also applies to all (equal-time) correlation functions of diagonal operators, and hence our FDS results translate to the (2+1)D \mathbb{Z}_N LGT.

Conclusion & Outlook.— In this work, we introduced *field digitization scaling* as an extension of the standard scaling paradigm by relating theories with different truncations in the number of field states. We thus take first steps towards a comprehensive RG framework for field-regularized models, with the ultimate goal of controlling continuum limits in corresponding classical and quantum simulations.

We initiate this program at the hand of numerical tensor-network calculations of one of the best studied 2D classical-statistical models, and, while some of the here presented results are specific to this case (e.g., the BKT nature of the critical point T_L), we expect our results to be relevant for a wider range of models also in higher dimensions. In this context, an immediate follow-up question addresses FDS in (2+1)D

N -state quantum clock models, where emergent $U(1)$ symmetries are expected and display an intriguing interplay with dangerously irrelevant clock perturbations [67, 68].

Beyond fundamental interest, our results have practical implications for quantum simulations of QFTs – where we are especially interested in the case of lattice gauge theories – as a digitization of the local Hilbert space in presence of continuous symmetry groups poses an outstanding challenge. In this context, a detailed understanding of FDS may thus open the door for

quantitative resource estimates for reaching the continuum limit with quantum hardware.

Acknowledgements.— This work is supported by the European Union’s Horizon Europe research and innovation program under Grant Agreement No. 101113690 (PASQuanS2.1), the ERC Starting grant QARA (Grant No. 101041435), the EU-QUANTERA project TNiSQ (N-6001), the Austrian Science Fund (FWF) (Grant No. DOI 10.55776/COE1). The computational results presented here have been achieved using the LEO HPC infrastructure of the University of Innsbruck.

-
- [1] S. Sachdev, *Quantum Phases of Matter* (Cambridge University Press, Cambridge, 2023).
 - [2] S. Weinberg, *The Quantum Theory of Fields*, Vol. 2 (Cambridge university press, 1995).
 - [3] F. Assaad and H. Evertz, in *Computational Many-Particle Physics*, edited by H. Fehske, R. Schneider, and A. Weiße (Springer Berlin Heidelberg, Berlin, Heidelberg, 2008) pp. 277–356.
 - [4] I. Montvay and G. Münster, *Quantum fields on a lattice* (Cambridge University Press, 1994).
 - [5] R. Orús, *Nat Rev Phys* **1**, 538 (2019).
 - [6] J. I. Cirac, D. Pérez-García, N. Schuch, and F. Verstraete, *Rev. Mod. Phys.* **93**, 045003 (2021).
 - [7] C. W. Bauer, Z. Davoudi, A. B. Balantekin, T. Bhattacharya, M. Carena, W. A. De Jong, P. Draper, A. El-Khadra, N. Gemelke, M. Hanada, *et al.*, *PRX Quantum* **4**, 027001 (2023).
 - [8] A. Di Meglio, K. Jansen, I. Tavernelli, C. Alexandrou, S. Arunachalam, C. W. Bauer, K. Borras, S. Carrazza, A. Crippa, V. Croft, *et al.*, *PRX Quantum* **5**, 037001 (2024).
 - [9] H. J. Rothe, *Lattice gauge theories: an introduction* (World Scientific Publishing Company, 2012).
 - [10] J. Cardy, *Scaling and Renormalization in Statistical Physics*, Cambridge Lecture Notes in Physics (Cambridge University Press, Cambridge, 1996).
 - [11] S. P. Jordan, K. S. M. Lee, and J. Preskill, *Science* **336**, 1130 (2012).
 - [12] N. Klco and M. J. Savage, *Phys. Rev. A* **99**, 052335 (2019).
 - [13] C. Delcamp and A. Tilloy, *Phys. Rev. Research* **2**, 033278 (2020).
 - [14] Y. Meurice, R. Sakai, and J. Unmuth-Yockey, *Rev. Mod. Phys.* **94**, 025005 (2022).
 - [15] J. Bender, E. Zohar, A. Farace, and J. I. Cirac, *New J. Phys.* **20**, 093001 (2018).
 - [16] A. Alexandru, P. F. Bedaque, S. Harmalkar, H. Lamm, S. Lawrence, N. C. Warrington, and N. Collaboration), *Phys. Rev. D* **100**, 114501 (2019).
 - [17] D. C. Hackett, K. Howe, C. Hughes, W. Jay, E. T. Neil, and J. N. Simone, *Phys. Rev. A* **99**, 062341 (2019).
 - [18] D. González-Cuadra, T. V. Zache, J. Carrasco, B. Kraus, and P. Zoller, *Phys. Rev. Lett.* **129**, 160501 (2022).
 - [19] H. Lamm, Y.-Y. Li, J. Shu, Y.-L. Wang, and B. Xu, *Phys. Rev. D* **110**, 054505 (2024).
 - [20] E. J. Gustafson, Y. Ji, H. Lamm, E. M. Murairi, S. O. Perez, and S. Zhu, *Phys. Rev. D* **110**, 034515 (2024).
 - [21] T. Byrnes and Y. Yamamoto, *Phys. Rev. A* **73**, 022328 (2006).
 - [22] E. Zohar and M. Burrello, *Phys. Rev. D* **91**, 054506 (2015).
 - [23] Z. Davoudi, I. Raychowdhury, and A. Shaw, *Phys. Rev. D* **104**, 074505 (2021).
 - [24] A. Ciavarella, N. Klco, and M. J. Savage, *Phys. Rev. D* **103**, 094501 (2021).
 - [25] M. L. Rhodes, M. Kreshchuk, and S. Pathak, *PRX Quantum* **5**, 040347 (2024).
 - [26] L. Ebner, A. Schäfer, C. Seidl, B. Müller, and X. Yao, *Phys. Rev. D* **110**, 014505 (2024).
 - [27] A. J. Buser, H. Gharibyan, M. Hanada, M. Honda, and J. Liu, *J. High Energ. Phys.* **2021**, 1 (2021).
 - [28] G. Bergner, M. Hanada, E. Rinaldi, and A. Schäfer, *J. High Energ. Phys.* **2024**, 1 (2024).
 - [29] T. V. Zache, D. González-Cuadra, and P. Zoller, *Phys. Rev. Lett.* **131**, 171902 (2023).
 - [30] T. Hayata and Y. Hidaka, *J. High Energ. Phys.* **2023**, 1 (2023).
 - [31] T. Hayata and Y. Hidaka, *Phys. Rev. D* **111**, 034513 (2025).
 - [32] A. N. Ciavarella and C. W. Bauer, *Phys. Rev. Lett.* **133**, 111901 (2024).
 - [33] S. Chandrasekharan and U.-J. Wiese, *Nucl. Phys. B* **492**, 455 (1997).
 - [34] U.-J. Wiese, *Phil. Trans. R. Soc. A* **380**, 20210068 (2022).
 - [35] V. Kasper, F. Hebenstreit, M. K. Oberthaler, and J. Berges, *Phys. Lett. B* **760**, 742 (2016).
 - [36] T. V. Zache, M. Van Damme, J. C. Halimeh, P. Hauke, and D. Banerjee, *Phys. Rev. D* **106**, L091502 (2022).
 - [37] J. C. Halimeh, L. Homeier, A. Bohrdt, and F. Grusdt, *PRX Quantum* **5**, 030358 (2024).
 - [38] G. Calliari, M. Di Liberto, H. Pichler, and T. V. Zache, *PRX Quantum* **6**, 030304 (2025).
 - [39] R. Joshi, M. Meth, J. C. Louw, J. J. Osborne, K. Mato, M. Ringbauer, and J. C. Halimeh, (2025), 10.48550/arXiv.2507.12589.
 - [40] H. Singh and S. Chandrasekharan, *Phys. Rev. D* **100**, 054505 (2019).
 - [41] T. Bhattacharya, A. J. Buser, S. Chandrasekharan, R. Gupta, and H. Singh, *Phys. Rev. Lett.* **126**, 172001 (2021).
 - [42] S. Maiti, D. Banerjee, S. Chandrasekharan, and M. K. Marinkovic, *Phys. Rev. Lett.* **132**, 041601 (2024).
 - [43] J. Ingoldby, M. Spannowsky, T. Sytchenko, and S. Williams, *Phys. Rev. D* **110**, 096016 (2024).
 - [44] G. Ortiz, E. Cobanera, and Z. Nussinov, *Nucl. Phys. B* **854**, 780 (2012).
 - [45] In this work, we are interested in the large N behavior; the detailed universal aspects of N -state clock models differ for small $N < 5$ [54].
 - [46] S. Elitzur, R. B. Pearson, and J. Shigemitsu, *Phys. Rev. D* **19**, 3698 (1979).
 - [47] H. Ueda, K. Okunishi, K. Harada, R. Krémár, A. Gendiar, S. Yunoki, and T. Nishino, *Phys. Rev. E* **101**,

- 062111 (2020).
- [48] C. Chatelain, *J. Stat. Mech.* **2014**, P11022 (2014).
 - [49] V.L. Berezinskii, *Soviet Physics-JETP* **32**, 493 (1971).
 - [50] V.L. Berezinskii, *Soviet Physics-JETP* **34**, 610 (1972).
 - [51] J. M. Kosterlitz, *J. Phys. C: Solid State Phys.* **7**, 1046 (1974).
 - [52] M. T. Fishman, L. Vanderstraeten, V. Zauner-Stauber, J. Haegeman, and F. Verstraete, *Phys. Rev. B* **98**, 235148 (2018).
 - [53] P. B. Wiegmann, *J. Phys. C: Solid State Phys.* **11**, 1583 (1978).
 - [54] Z.-Q. Li, L.-P. Yang, Z. Y. Xie, H.-H. Tu, H.-J. Liao, and T. Xiang, *Phys. Rev. E* **101**, 060105 (2020).
 - [55] In this work, we do not investigate the second BKT transition at $T = T_H$, whose behavior is essentially independent of N .
 - [56] G. Li, K. H. Pai, and Z.-C. Gu, *Phys. Rev. Research* **4**, 023159 (2022).
 - [57] S. Kehrein, *Nucl. Phys. B* **592**, 512 (2001).
 - [58] In this work we use the critical temperatures $T_L(N)$ numerically determined in Ref. [56].
 - [59] By comparing our results Eq. (5) to the derived ξ behavior, we infer $C \approx |t|/N$, which can also be interpreted as an N -dependent UV initialization of $g_L(T, N) \propto \sqrt{|t|/N}$.
 - [60] L. Tagliacozzo, Thiago. R. De Oliveira, S. Iblisdir, and J. I. Latorre, *Phys. Rev. B* **78**, 024410 (2008).
 - [61] F. Pollmann, S. Mukerjee, A. Turner, and J. E. Moore, *Phys. Rev. Lett.* **102**, 255701 (2009).
 - [62] Due to the truncation in χ , the scaling variable $x = x(\xi)$ cannot be a constant in the whole critical region, but rather it quantifies the proximity to the CP.
 - [63] F. Verstraete, M. M. Wolf, D. Perez-Garcia, and J. I. Cirac, *Phys. Rev. Lett.* **96**, 220601 (2006).
 - [64] D. Horn, M. Weinstein, and S. Yankielowicz, *Phys. Rev. D* **19**, 3715 (1979).
 - [65] C. Castelnovo and C. Chamon, *Phys. Rev. B* **77**, 054433 (2008).
 - [66] For simplicity, here we state the result for an infinite plane, where the ground state is unique.
 - [67] P. Patil, H. Shao, and A. W. Sandvik, *Phys. Rev. B* **103**, 054418 (2021).
 - [68] H. Shao, W. Guo, and A. W. Sandvik, *Science* **352**, 213 (2016).
 - [69] J. Naumann, E. L. Weerda, M. Rizzi, J. Eisert, and P. Schmoll, *SciPost Phys. Lect. Notes*, 86 (2024).
 - [70] Our standard implementation of the CTMRG algorithm closely follows Ref. [69], and our isotropic code is inspired by Ref. [52].

APPENDIX

Appendix A: Tensor-network simulations

In this Appendix we provide details on our numerical simulations. We numerically investigate the 2D classical N -state clock model [Eq. (1)] with an infinite 2D tensor network by encoding the partition function Z in an iPEPS state $|\psi\rangle$ [63].

To derive an explicit form of $|\psi\rangle$, we start from a product state $\otimes_i |+\rangle$, with $|+\rangle = \sum_{n=0}^{N-1} |n\rangle$, and then apply the operator $\exp\{-\beta h_{ij}/2\}$ on all bonds between two nearest-neighbor tensors on sites i, j , with β the inverse temperature. Here, $h_{ij} = -(Z_i Z_j^\dagger + Z_i^\dagger Z_j)/2$ are local (two-site) contributions to the Hamiltonian of the N -state clock model $H_N = \sum_{\langle ij \rangle} h_{ij}$, where $Z_i = e^{i\vartheta_i}$, with $\vartheta_i = 2\pi n_i/N$ ($n_i = 0, \dots, N-1$), and $J = 1$. Using $Z_i^N = 1$, we decompose the exponential as

$$e^{-\frac{\beta}{2} h_{ij}} = \begin{array}{|c|} \hline \begin{array}{c} s'_i \\ \hline \text{white tensor} \\ \hline s_i \end{array} \\ \hline \end{array} = \begin{array}{|c|} \hline \begin{array}{c} s'_i \\ \hline \text{blue tensor} \\ \hline s_i \end{array} \\ \hline \end{array} \quad (A1)$$

where the white tensor on the RHS represents $\sqrt{c_m(\beta/2)}(Z^m)_{s_i s'_i}$, and the blue tensor is its Hermitian conjugate, with real coefficients

$$c_m \left(\frac{\beta}{2} \right) = \frac{1}{N} \sum_{k=0}^{N-1} \cos \left(\frac{2\pi k m}{N} \right) e^{-\frac{\beta}{2} \cos \left(\frac{2\pi k}{N} \right)}. \quad (A2)$$

Here the labels s_i, s'_i indicate the matrix element (s_i, s'_i) in the matrix representation of the operator (see App. C). We thus define the local PEPS tensor A_ψ for $|\psi\rangle$ by applying the blue and white tensors to the (product state) PEPS A_+ that corresponds to $|+\rangle$, as shown in Fig. S1(a).

Due to the asymmetry between blue and white tensors in the decomposition Eq. (A1), A_ψ is not symmetric under spatial rotations, in apparent conflict with the rotational invariance of H_N . It is useful to restore this symmetry as follows. We first rewrite $\sqrt{c_m}(Z^\dagger)^m = U_{N-m, m'} \cdot \sqrt{c_{m'}} Z^{m'}$, with the unitary $U_{m, m'} = \delta_{m, N-m'}$, which can be further decomposed as $U = O \cdot O^T$. This allows us to gauge the PEPS according to

$$\begin{array}{|c|} \hline \text{blue tensor} \\ \hline \end{array} = \begin{array}{|c|} \hline \text{white tensor} \\ \hline \end{array} U = \begin{array}{|c|} \hline \text{white tensor} \\ \hline \end{array} O^T = \begin{array}{|c|} \hline \text{green tensor } V \\ \hline \end{array}. \quad (A3)$$

We thus obtain the operator V (green tensor), which corresponds to a symmetric decomposition of $\exp\{-\beta h_{ij}/2\}$. By applying V on the tensor A_+ , as shown in Fig. S1(b), we obtain the desired rotational-invariant representation B_ψ of $|\psi\rangle$.

Since we mainly focus on local observables, we can restrict ourselves to a single site and approximate the contraction of the infinite tensor network with environment tensors (ETs): given the rotational symmetry, we only use a single corner transfer matrix C and one half-row/column transfer matrix T , which we optimize using the isotropic CTMRG algorithm [52, 69][70].

In our numerics we further impose ferromagnetic boundary conditions as follows. We first run CTMRG for increasingly small bias magnetic fields $h \neq 0$, obtained by adding to H_N the term $h(Z_i + Z_i^\dagger)$ to bias the

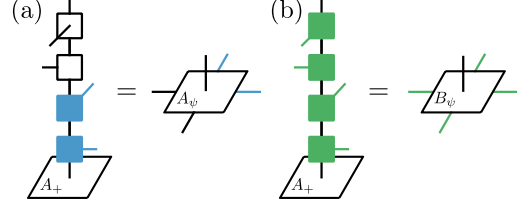


Figure S1. **Tensor-network encoding of the state $|\psi\rangle$.** (a) The tensor A_ψ is obtained by applying on A_+ (representing $|+\rangle$) the operators $\sqrt{c_m} Z^{(\dagger)m}$ [white (blue) tensor] in two spatial directions each. (b) A rotational-invariant encoding B_ψ is instead obtained by symmetrically applying the tensors V [green tensor].

symmetry-broken phase towards the angle along $\vartheta = 0$. We then use the resulting ETs as initial Ansätze for the successive optimizations at smaller h . Specifically, we compute ETs for $h = 10^{-2}, 10^{-4}$ with a convergence parameter $\epsilon = 10^{-5}$, where ϵ is the maximal difference between the values of the (diagonal) matrix C in two subsequent steps. In the end, we run one final CTMRG with initial ETs optimized at the smallest $h \neq 0$ for the $h = 0$ case with $\epsilon = 10^{-8}$.

Having determined both A_ψ and the ETs C, T , we evaluate local observables. The magnetization M is given by the single-site expectation value $M = \langle Z + Z^\dagger \rangle / 2$. By contracting T with itself we also build a row/column transfer matrix from which we compute the correlation length $\xi = 1 / \ln(\lambda_1 / \lambda_2)$, with λ_1, λ_2 the two largest eigenvalues. In our numerical analysis we discarded clearly deviating data points.

Appendix B: Functional form of the correlation length ξ from the RG flow equations

In this Appendix we elaborate on the RG calculations used to derive the functional form of the correlation length ξ . In the action S_N Eq. (3) for $T < T_H$ the term $\cos(\sqrt{2}\phi)$ becomes irrelevant, thus allowing us to map S_N to the standard sG action [57]

$$S_{\text{sG}} = \int d^2x \left\{ \frac{1}{2} (\partial_\mu \varphi)^2 + \frac{u}{\alpha^2} \cos(\beta_{\text{sG}} \varphi) \right\}, \quad (A1)$$

using the substitution $N\theta\sqrt{2} \rightarrow \beta_{\text{sG}}\varphi$, as well as the parameter identifications $\beta_{\text{sG}}^2 = 2\pi N^2/K$, and $u = g_L(T, N)/2\pi$.

Close to the CP $\beta_{\text{sG}}^2 \approx 8\pi$, the sG RG flow equations are given by $d\tilde{\beta}^2/d\ln\Lambda = 4u^2$, $du/d\ln\Lambda = (\tilde{\beta}^2 - 2)u$, with $\tilde{\beta}^2 = \beta_{\text{sG}}^2/4\pi$, while $\Lambda = e^{-l}$ defines the (inverse) length scale [57]. Furthermore, at the CP the Luttinger parameter $K_L(N) = N^2/4$, and using the expansion $K = K_L + \delta K$, we find $d = 1 - \tilde{\beta}^2/2 = 4\delta K/N^2$, with $0 < d \ll 1$ in the gapped phase close to the CP. We further assume $u > 0$. Rewriting the RG equations in terms of the variables $z_{1/2} = u \pm d$, as $dz_{1/2}/d\ln\Lambda = \mp z_{1/2}(z_1 + z_2)$ and using that $z_1 \cdot z_2 = u^2 - d^2 = C(N, T)$ is a constant of the flow, we obtain $dz_1/d\ln\Lambda = -(z_1^2 + C)$. The solution is $z_1(l) = \sqrt{C} \tan(\sqrt{C}l + c_1)$, with c_1

a constant. We can then rewrite $u(l) = (z_1 + C/z_1)/2$, and fix $c_1 = \arctan\{(\varepsilon + \sqrt{\varepsilon^2 - C}/C)/\sqrt{C}\}$ from the initial value $u(0) = \varepsilon$. At the start of the RG flow, both $u(0), d(0) \ll 1$; due to the closeness to the CP we further assume $1 \gg u(0) \gg d(0) > 0$, i.e., $C \approx \varepsilon \ll 1$. Hence, $c_1 \approx \arctan(\varepsilon/\sqrt{C}) \approx \pi/4$. Consider the flow parameter l^* at which $u(l^*) = 1$, which equals

$$l^* = \frac{1}{\sqrt{C}} \left(-c_1 + \arctan \left[\frac{1+\sqrt{1-C}}{\sqrt{C}} \right] \right) \approx \frac{\pi}{4\sqrt{C}}. \quad (\text{A2})$$

This identifies the characteristic correlation length as $\xi = e^{l^*}$, equal to $\xi \propto \exp\{\pi/(4\sqrt{C})\}$.

In the gapped region, we extrapolate our numerical results to $\chi \rightarrow \infty$ with a fit in $1/\chi$ (for $\chi \geq 70$), and consider only temperatures for which ξ_∞ has a relative error of at most 3.5% ($T \leq T_L - \Delta T$, with $\Delta T \approx 0.02-0.03$). From the extrapolated data we empirically find that $C \approx |t|/N$, and the overall prefactor $\xi_0(N) \approx \log(2)/N^{1.5}$.

Appendix C: Connection to a (2+1)D \mathbb{Z}_N LGT

Here, we extend a known result from the deformed toric code model for $N = 2$ [65] and we prove that Eq. (9) is the ground state (GS) of a (2+1)D locally \mathbb{Z}_N -symmetric quantum Hamiltonian. We first consider an infinite 2D lattice [see Fig. 5(b)], with degrees of freedom located on the links. While in the main text we focus on one type of boundary conditions, the following proof is valid for general 2D topologies/boundary conditions.

We first define the N -dimensional “clock” operator $Z = \sum_{n=0}^{N-1} \omega^n |n\rangle\langle n|$ and the cyclic “shift” operator $X = \sum_{n=0}^{N-1} |(n+1) \bmod N\rangle\langle n|$, with local basis states $|n\rangle$, $n = 0, \dots, N-1$ and $\omega = e^{\frac{2\pi i}{N}}$. These operators fulfill the commutation relations $XZ = \omega^* ZX$ and $X^\dagger Z = \omega Z X^\dagger$, as well as $Z^N = X^N = 1$. From the main text, we recall the Gauss’ law $G_s(\{Z_l\})$ and plaquette operators $U_p(\{X_l\})$; from the above commutation relations, it is easy to check that $[U_p, G_s] = 0$. We further define the Abelian group $G = \{g\}$ with $g = \prod_p (U_p)^{n_p}$.

Consider now the Hamiltonian

$$H = \lambda_0 H_0 + \lambda_1 H_{\text{LGT}}, \quad (\text{A1})$$

where $H_0 = -\sum_s (G_s + G_s^\dagger)/2$ and H_{LGT} is given in Eq. (8), with the operators

$$D_p^{(\prime)}(\beta) = e^{-\frac{\beta}{4} [d_N^{(\prime)*} \sum_{l=1}^2 Z_{p,l} + d_N^{(\prime)} \sum_{l=3}^4 Z_{p,l} + \text{H.c.}]}, \quad (\text{A2})$$

where $d_N = 1 - \omega = d_N^*$, and $\lambda_0, \lambda_1 > 0$ are arbitrary couplings. For $\lambda_0 \rightarrow \infty$ we impose the Gauss’ law constraint as $G_s = 1, \forall s$, while in the limit $\beta \rightarrow 0$ H reduces to the well-known \mathbb{Z}_N toric code [64], up to an overall energy shift.

Our goal is to prove that the state

$$|\psi\rangle = \sum_\alpha \frac{\psi_\alpha}{\sqrt{Z_\alpha}} \sum_{g \in G} e^{\frac{\beta}{2} \sum_i \frac{1}{2} (Z_i + Z_i^\dagger)} g |\psi_\alpha\rangle, \quad (\text{A3})$$

is the ground state of H , where $\{|\psi_\alpha\rangle\}$ form a minimal, non-unique set of reference configurations, from which

under the action of G the full Hilbert space basis can be generated, closely following the discussion in Ref. [65] but now for \mathbb{Z}_N . Here, α labels the topological sectors of the \mathbb{Z}_N -toric code in non-trivial topologies, with ψ_α the weight of the normalized wavefunction in each sector, i.e., $\sum_\alpha |\psi_\alpha|^2 = 1$, and Z_α the partition function, such that $\langle \psi | \psi \rangle = 1$.

We first show that $|\psi\rangle$ is a GS to $H_{\text{LGT}} = \sum_p Q_p(\beta)$, with

$$Q_p(\beta) = \frac{1}{2} (D_p(\beta) + D_p'(\beta) - U_p - U_p^\dagger). \quad (\text{A4})$$

Using the commutation relations of X and Z , and the fact that $U_p^{(\dagger)} g \in G$, direct computation shows that $|\psi\rangle$ is annihilated by the operator $Q_p(\beta)$ and thus by H_{LGT} , so it is an eigenstate with eigenvalue zero. To show that $|\psi\rangle$ is also a GS, it is therefore sufficient to prove that Q_p is lower-bounded by zero. To do this, we first simplify the problem by considering conserved charges of Q_p , namely $Z_1^\dagger Z_2 = c_1, Z_2^\dagger Z_3^\dagger = c_2, Z_4 Z_1 = c_4$, with $c_m = e^{2\pi i p_m / N}$ and $p_m = 0, \dots, N-1$. It follows that Q_p is block diagonal in the corresponding subsectors, with blocks $\tilde{Q}_p = (\tilde{D}_p + \tilde{D}_p' - X - X^\dagger)/2$, where $\tilde{D}_p^{(\prime)} = \exp\{-\beta(d_N^{(\prime)*} cZ + \text{H.c.})/4\}$, with $c = 1 + c_1 + c_1 c_2 + c_4^* \in \mathbb{C}$, while $U_p^{(\dagger)} = X^{(\dagger)}$. Note that we dropped the label 1 in $Z_1^{(\dagger)}$. We thus find that

$$\tilde{Q}_p = \frac{1}{2} \sum_{n=0}^{N-1} [f_n |n\rangle\langle n| - |n\rangle\langle n-1| - |n\rangle\langle n+1|] \quad (\text{A5})$$

is a real symmetric operator with

$$f_n = e^{-\frac{\beta}{4} [\omega^n d_N^* c + \text{c.c.}]} + e^{-\frac{\beta}{4} [\omega^n d_N c + \text{c.c.}]} \geq 0, \quad (\text{A6})$$

and $|N\rangle \equiv |0\rangle, |-1\rangle \equiv |N-1\rangle$. To show that Q_p is positive-semidefinite, we now calculate $x^T \tilde{Q}_p x, \forall x = (x_0, \dots, x_{N-1})^T \in \mathbb{R}^N$. Explicitly,

$$x^T \tilde{Q}_p x = \frac{1}{2} \sum_{n=0}^{N-1} [x_n^2 f_n - (x_n x_{n+1} + x_{n-1} x_n)], \quad (\text{A7})$$

with $x_N \equiv x_0$ and $x_{-1} \equiv x_{N-1}$. Rewriting $f_n = g_n + 1/g_{n-1}$, with

$$g_n = e^{-\frac{\beta}{4} (c\omega^n + \text{c.c.})} / e^{-\frac{\beta}{4} (c\omega^{n+1} + \text{c.c.})} \geq 0 \quad (\text{A8})$$

and shifting indices of selected terms ($n \rightarrow n+1$) gives

$$x^T \tilde{Q}_p x = \frac{1}{2} \sum_{n=0}^{N-1} \left(x_n \sqrt{g_n} - \frac{x_{n+1}}{\sqrt{g_n}} \right)^2 \geq 0. \quad (\text{A9})$$

To summarize, \tilde{Q}_p and hence also Q_p is lower-bounded by zero, which implies that $|\psi\rangle$ is a GS of H_{LGT} .

Finally, to show that $|\psi\rangle$ is also the GS of H_0 , recall that for general topologies $|\psi_\alpha\rangle$ in Eq. (A3) are reference configurations in the different topological sectors of the \mathbb{Z}_N -toric code, which all fulfill $G_s = 1, \forall s$. Since $[G_s^{(\dagger)}, g] = 0 \forall g$, the application of g cannot modify the sector, and $|\psi\rangle$ is a GS of H_0 . Thus, the state $|\psi\rangle$ is a ground state of any combination of the two Hamiltonians H_0, H_{LGT} , and as such of H .

For an infinite system (with trivial boundaries), as discussed in the main text, the GS is unique. In this case, we choose a trivial reference state $|\psi_{\alpha'}\rangle = \otimes_l |0\rangle$ (i.e., $\psi_\alpha = \delta_{\alpha, \alpha'}$). We next introduce the variable $e^{i\vartheta_p}$

on the plaquette p , and, for a given configuration $\{\vartheta_p\}$, the value of Z_l on the link between two plaquettes p, p' is uniquely determined as $Z_l \equiv e^{i(\vartheta_p - \vartheta_{p'})}$ (see also Ref. [64]), and as such we rewrite $\sum_l (Z_l + Z_l^\dagger)/2 = \sum_{\langle p, p' \rangle} \cos(\vartheta_p - \vartheta_{p'})$. By inserting these relations in Eq. (A3), we obtain Eq. (9). This state can be directly encoded in a 2D iPEPS tensor network, and it is indeed the state we use in our numerical simulations (see App. A).